Interactions Between Tropical Convection and Its Embedding Environment: An Energetics Analysis of a 2-D Cloud Resolving Simulation

Xiaofan Li[1,2], C.-H. Sui, K.-M. Lau

NASA/Goddard Space Flight Center, Greenbelt, Maryland

Submitted to *J. Atmos. Sci.*

August, 1999

[1]Current affiliation: SM & A Corporation, Arlington, Virginia

[2]Corresponding author address: Dr. X. Li, SM & A Corporation, NASA/GSFC, Code 913, Greenbelt, MD 20771 < *email* > xli@climate.gsfc.nasa.gov

Abstract

The phase relation between the perturbation kinetic energy (K') associated with the tropical convection and the horizontal-mean moist available potential energy ($\overline{P}$) associated with environmental conditions is investigated by an energetics analysis of a numerical experiment. This experiment is performed using a 2-D cloud resolving model forced by the TOGA-COARE derived vertical velocity. The imposed upward motion leads to a decrease of $\overline{P}$ directly through the associated vertical advective cooling, and to an increase of K' directly through cloud related processes, feeding the convection. The maximum K' and its maximum growth rate lags and leads, respectively, the maximum imposed large-scale upward motion by about 1-2 hours, indicating that convection is phase locked with large-scale forcing. The dominant life cycle of the simulated convection is about 9 hours, whereas the time scales of the imposed large-scale forcing are longer than the diurnal cycle.

In the convective events, maximum growth of K' leads maximum decay of the perturbation moist available potential energy (P') by about 3 hours through vertical heat transport by perturbation circulation, and perturbation cloud heating. Maximum decay of P' leads maximum decay of $\overline{P}$ by about one hour through the perturbation radiative processes, the horizontal-mean cloud heating, and the large-scale vertical advective cooling. Therefore, maximum gain of K' occurs about 4-5 hours before maximum decay of $\overline{P}$.

1. Introduction

Tropical convection occurs as a result of release of unstable energy of its embedding environment. The large-scale environment provides favorable thermal and moisture conditions for convection occurrence and development, on one hand, and on the other hand, it is adjusted by redistributing vertical thermal, moisture, and momentum structures through the convection. Such interaction allows us to use environmental conditions to estimate the properties of the convection such as the precipitation, which is a cumulus parameterization. Since the environmental time scales (a few days and longer) are much longer than the convective time scales (a few hours and shorter), the rate of production of available potential energy by the large-scale processes is nearly balanced by the rate of consumption of the available potential energy by the convection (Manabe and Strickler 1964). This quasi-equilibrium concept is the basic premise of the cumulus parameterization scheme proposed by Arakawa and Schubert (1974). The decrease of convective available potential energy (CAPE) that measures the thermal and moisture conditions of the environment often coincides with the convection development so that the CAPE and rain rate are negatively correlated (e.g., Thompson et al. 1979; Cheng and Yanai 1989; Wang and Randall 1994; Xu and Randall 1998). The phase relation between the CAPE and rainfall may be related to the coupling between environmental dynamic and thermodynamic fields (Cheng and Yanai 1989).

Recently, the phase difference between the CAPE and rainfall has been found as the evidence for relaxing the quasi-equilibrium assumption in cumulus parameterization (e.g., Betts and Miller, 1986; Randall and Pan 1993). The minimum CAPE occurs a few hours [e.g., 3 hours in GATE (Global Atmospheric Research Program Atlantic Tropical Experiment); 6 hours in (TOGA-COARE) Tropical Oceans Global Atmosphere Coupled Ocean-Atmosphere Response Experiment] after maximum rainfall. Such a phase lag is also demonstrated by Xu and Randall (1998) in their 2-D cloud resolving simulations. Xu and Randall (1998) interpreted the maximum phase lag as the adjustment time scale from disequilibrium to quasi-equilibrium states in the presence of time-varying large-scale forcing.

In this study, the physical processes responsible for such phase relation are examined through the analysis of energy conversion processes between available potential energy and kinetic energy in a 2-D cloud resolving simulation. We, first, establish the phase relation between available potential energy and kinetic energy, and use a set of energetics equations (section 2) to examine the essential physical processes determining the phase relation (section 3). The phase relation is discussed in Section 4, and the conclusion is given in section 5.

2. Formulations for model, energetics, and CAPE

2a. Model

The cloud resolving model was originally developed by Soong and Ogura (1980), Soong and Tao (1980), and Tao and Simpson (1993), for studying deep convective response to the specified large-scale forcing. A 2-D version of the model used by Sui et al. (1998) and modified by Li et al. (1999) is used in this study. The governing equations with an anelastic approximation can be expressed as follows:

$$\frac{\partial u'}{\partial x} + \frac{1}{\overline{\rho}}\frac{\partial}{\partial z}\overline{\rho}w' = 0, \tag{1}$$

$$\frac{\partial u'}{\partial t} = -\frac{\partial}{\partial x}(u'\overline{u}^o + \overline{u}^o u' + u'u') - \frac{1}{\overline{\rho}}\frac{\partial}{\partial z}\overline{\rho}(w'\overline{u}^o + \overline{w}^o u' + w'u' - \overline{w'u'})$$
$$-c_p\frac{\partial}{\partial x}(\overline{\theta}\pi') + D_u - \overline{D}_u, \tag{2}$$

$$\frac{\partial w'}{\partial t} = -\frac{\partial}{\partial x}(u'\overline{w}^o + \overline{u}^o w' + u'w') - \frac{1}{\overline{\rho}}\frac{\partial}{\partial z}\overline{\rho}(w'\overline{w}^o + \overline{w}^o w' + w'w' - \overline{w'w'})$$
$$-c_p\frac{\partial}{\partial z}(\overline{\theta}\pi') + g(\frac{\theta'}{\theta_b} + 0.61q'_v - q'_l) + D_w - \overline{D}_w, \tag{3}$$

$$\frac{\partial \theta}{\partial t} = -\frac{\partial(u'\theta')}{\partial x} - \overline{u}^o\frac{\partial \theta'}{\partial x} - \frac{1}{\overline{\rho}}\frac{\partial}{\partial z}\overline{\rho}w'\theta' - \overline{w}^o\frac{\partial \theta'}{\partial z} - w'\frac{\partial \overline{\theta}}{\partial z}$$

$$+\frac{1}{\pi c_p}Q_{cn}+\frac{1}{\pi c_p}Q_R-\overline{u}^o\frac{\partial\overline{\theta}^o}{\partial x}-\overline{w}^o\frac{\partial\overline{\theta}}{\partial z}+D_\theta, \tag{4}$$

$$\frac{\partial q_v}{\partial t}=-\frac{\partial(u'q_v')}{\partial x}-\overline{u}^o\frac{\partial q_v'}{\partial x}-\frac{1}{\overline{\rho}}\frac{\partial}{\partial z}\overline{\rho}w'q_v'-\overline{w}^o\frac{\partial q_v'}{\partial z}-w'\frac{\partial\overline{q}_v}{\partial z}$$
$$-(c-e+d-s)-\overline{u}^o\frac{\partial\overline{q_v}^o}{\partial x}-\overline{w}^o\frac{\partial\overline{q}_v}{\partial z}+D_{q_v}, \tag{5}$$

$$\frac{\partial C}{\partial t}=-\frac{\partial(uC)}{\partial x}-\frac{1}{\overline{\rho}}\frac{\partial}{\partial z}[\overline{\rho}(w-w_{TV})C]+S_C+D_C. \tag{6}$$

Here u, and w are zonal, and vertical wind components; θ and q_v are potential temperature and specific humidity respectively; $C=(q_c,q_r,q_i,q_s,q_g)$, q_c, q_r, q_i, q_s, and q_g are the mixing ratios of cloud water, rain, cloud ice, snow, and graupel, respectively; $\overline{\rho}$ is a mean air density which is a function of height only; w_{TV} is a terminal velocity which is zero for cloud water and ice; $\pi=(p/p_o)^\kappa$, $\kappa=\frac{R}{c_p}$, R is the gas constant, c_p is the specific heat of dry air at constant pressure p, and p_o=1000 mb; c, e, d, and s denote condensation, evaporation, deposition, and sublimation, respectively; $Q_{cn}=L_v(c-e)+L_s(d-s)+L_f(f-m)$ denotes the net latent heat release through phase changes among different cloud species, where f and m are fusion and melting, respectively; L_v, L_s, and L_f are heat coefficients due to phase changes; Q_R is the radiative heating rate due to convergence of net flux of solar and infrared radiative fluxes; S_C is source and sink of cloud content determined by microphyical processes; Ds are dissipation terms; overbar ($^-$) denotes a zonal-mean; subscript $_b$ denotes an initial value, which does not vary with time; superscript ^{o} denotes imposed observed variables in the model. More discussions about the model and the model responses to prescribed TOGA-COARE forcing are reported in Li et al. (1999).

2b. Energetics equations

The perturbation kinetic energy and zonal-mean and perturbation moist available potential energy are respectively defined by

$$K'=<\frac{\overline{(u')^2+(w')^2}}{2}>, \tag{7a}$$

$$\overline{P} =< \frac{\Gamma}{c_p}\frac{(\overline{h}-h_b)^2}{2} >, \tag{7b}$$

$$P' =< \frac{\Gamma}{c_p}\frac{\overline{(h')^2}}{2} >, \tag{7c}$$

where $h = c_pT + L_vq_v$; T is temperature; $\Gamma = -\kappa\theta(pT)^{-1}(\frac{\partial\theta_b}{\partial p} + \frac{L_v}{c_p\pi}\frac{\partial q_{vb}}{\partial p})^{-1}$, which is a parameter related to static stability; the angle bracket implies a vertical integration:

$$< () >= \int_{z_B}^{z_T} \overline{\rho}()dz. \tag{8}$$

Here z_B and z_T are the heights of bottom and top of the model, respectively. Note that the horizontal-mean moist available potential energy ($\overline{P}$) is different from the moist available energy (MAE) proposed by Lorenz (1978, 1979). The difference arises from the definition of h_b. Here, h_b is defined as a reference state, and is defined as the initial state (anelastic approximation), whereas the MAE is calculated based on the assumption that the parcel conserves its equivalent potential temperature in the Lagrangian frame, and equivalently, h_b varies with time as the surface temperature and moisture vary. The vertical component of the moist available energy is a generalization of CAPE (Randall and Wang 1992). In the following derivations of energetics equations, the dissipation terms are excluded.

An equation for the perturbation kinetic energy (K') can be derived by multiplying (2) by u' and (3) by w' and applying zonal-mean and the integration defined by (8) on the resulting equation:

$$\frac{\partial K'}{\partial t} = C(\overline{K}, K') + C(P', K') + G_{q_v}(K') + G_{q_l}(K'), \tag{9}$$

where

$$C(\overline{K}, K') = - < \overline{u'w'}\frac{\partial \overline{u}^o}{\partial z} > - < \overline{w'w'}\frac{\partial \overline{w}^o}{\partial z} >, \tag{9a}$$

$$C(P', K') =< g\frac{\overline{w'T'}}{T_b} >, \tag{9b}$$

$$G_{q_v}(K') =< 0.61g\overline{w'q_v'} >, \tag{9c}$$

$$G_{q_l}(K') = - < g\overline{w'q_l'} > . \tag{9d}$$

Here, $C(\overline{K}, K')$ is the conversion between $\overline{K}$ and K' through covariance between perturbation zonal wind and vertical velocity under vertical shear of imposed horizontal-mean zonal wind, and between perturbation vertical velocities under vertical shear of imposed horizontal-mean vertical velocity. $C(P', K')$ is the conversion between P' and K' through covariance between perturbation vertical velocity and temperature. $G_{q_v}(K')$ and $G_{q_l}(K')$ are the generation terms of K' through covariance between perturbation vertical velocity and specific humidity, and between perturbation vertical velocity and cloud mixing ratio, respectively.

To derive the equations for the zonal-mean and perturbation moist available potential energy, the following equation is formed by multiplying (4) by $c_p\pi$ and (5) by L_v and adding the resulting equations:

$$\frac{\partial h}{\partial t} = -\frac{\partial (u'h')}{\partial x} - \overline{u}^o \frac{\partial h'}{\partial x} - \frac{c_p \pi}{\overline{\rho}} \frac{\partial}{\partial z} \overline{\rho} w' \theta' - c_p \pi \overline{w}^o \frac{\partial \theta'}{\partial z}$$

$$- \frac{L_v}{\overline{\rho}} \frac{\partial}{\partial z} \overline{\rho} w' q_v' - L_v \overline{w}^o \frac{\partial q_v'}{\partial z} - c_p \pi w' \frac{\partial \overline{\theta}}{\partial z} - L_v w' \frac{\partial \overline{q}_v}{\partial z} + [(L_s - L_v)(d - s)$$

$$+ L_f (f - m)] + Q_R - \overline{u}^o \frac{\partial \overline{h}^o}{\partial x} - c_p \pi \overline{w}^o \frac{\partial \overline{\theta}}{\partial z} - L_v \overline{w}^o \frac{\partial \overline{q}_v}{\partial z}. \tag{10}$$

The equations for the zonal-mean moist available potential energy ($\overline{P}$) and the perturbation moist available potential energy (P') can be derived by multiplying (10) by $c_p^{-1}\Gamma(\overline{h} - h_b)$, and by $c_p^{-1}\Gamma h'$, and applying zonal-mean and the integration defined by (8) on the resulting equations:

$$\frac{\partial \overline{P}}{\partial t} = C(P', \overline{P}) + G_R(\overline{P}) + G_{cn}(\overline{P}) + C_h(\overline{K}, \overline{P}) + C_v(\overline{K}, \overline{P}), \tag{11}$$

$$\frac{\partial P'}{\partial t} = -C(P', \overline{P}) - C(P', K') + G_R(P') + G_{cn}(P') + G(P'), \tag{12}$$

where

$$C(P', \overline{P}) = - < \frac{\Gamma}{c_p} (\overline{h} - h_b)(c_p \pi \frac{\partial}{\overline{\rho} \partial z} \overline{\rho} \overline{w'\theta'} + L_v \frac{\partial}{\overline{\rho} \partial z} \overline{\rho} \overline{w' q_v'}) >, \tag{11a}$$

$$G_R(\overline{P}) = < \frac{\Gamma}{c_p} \overline{Q}_R (\overline{h} - h_b) >, \tag{11b}$$

$$G_{cn}(\overline{P}) =< \frac{\Gamma}{c_p}(\overline{h}-h_b)[(L_s-L_v)(\overline{d}-\overline{s})+L_f(\overline{f}-\overline{m})] >, \tag{11c}$$

$$C_h(\overline{K},\overline{P}) = - < \frac{\Gamma}{c_p}(\overline{h}-h_b)\overline{u}^o(c_p\pi\frac{\partial\overline{\theta}^o}{\partial x}+L_v\frac{\partial\overline{q}_v^o}{\partial x}) >, \tag{11d}$$

$$C_v(\overline{K},\overline{P}) = - < \frac{\Gamma}{c_p}(\overline{h}-h_b)\overline{w}^o(c_p\pi\frac{\partial\overline{\theta}}{\partial z}+L_v\frac{\partial\overline{q}_v}{\partial z}) >, \tag{11e}$$

$$G_R(P') =< \frac{\Gamma}{c_p}\overline{Q_R h'} >, \tag{12a}$$

$$G_{cn}(P') =< \frac{\Gamma}{c_p}\overline{h'[(L_s-L_v)(d-s)+L_f(f-m)]} >, \tag{12b}$$

$$\begin{aligned} G(P') = & - < \frac{gL_v}{c_pT_b}\overline{w'q_v'} > - < \frac{\Gamma}{c_p}\frac{\partial}{\overline{\rho}\partial z}[(\overline{h}-h_b)\overline{\rho}(\overline{h'w'})] > \\ & - < \frac{g\Gamma}{c_pT_b}(\frac{\overline{T}}{T_b}-1)\overline{h'w'} > - < \frac{g\Gamma}{c_pT_b}(\overline{h}-h_b)\overline{T'w'} > \\ & - < \frac{\Gamma}{2c_p}\frac{\partial}{\overline{\rho}\partial z}[\overline{\rho(\overline{w}^o+w')(h')^2}] > - < \frac{g\Gamma}{c_pT_b}\overline{(\overline{w}^o+w')T'h'} > . \end{aligned} \tag{12c}$$

Here, $C(P',\overline{P})$ is the conversion between P' and $\overline{P}$ through covariance between $\overline{h}-h_b$ and convergence of vertical flux of potential temperature and moisture. $G_R(\overline{P})$ and $G_{cn}(\overline{P})$ are the generation terms of $\overline{P}$ through covariances between $\overline{h}-h_b$ and horizontal-mean radiative heating, and between $\overline{h}-h_b$ and horizontal-mean heating due to phase change of the cloud contents respectively. $C_h(\overline{K},\overline{P})$ and $C_v(\overline{K},\overline{P})$ are the conversion between $\overline{K}$ and $\overline{P}$ through covariances between $\overline{h}-h_b$ and imposed horizontal temperature and moisture advections, and between $\overline{h}-h_b$ and the horizontal-mean vertical temperature and moisture advections by imposed vertical velocity respectively. $G_R(P')$ and $G_{cn}(P')$ are the generation terms of P' through covariances between h' and perturbation radiative heating, and between h' and perturbation heating due to phase changes of the cloud contents, respectively. $G(P')$ is the generation term of P'. Note that $C(\overline{P},P')+C(K',P')+G(P')$ causes changes of P' due to the vertical advection processes. The key steps to derive (9) and (12) can be found in Appendix.

2c. CAPE calculation

The CAPE can be calculated by

$$CAPE = g \int_{LFC}^{z_c} \frac{\theta_{pcl}(z) - \theta_{env}(z)}{\theta_{env}(z)} dz. \tag{13}$$

Here θ_{pcl} is the potential temperature of an air parcel lifted from z_B to z_T while not mixing with its environment (θ_{env}). The air parcel is lifted dry adiabatically until it becomes saturated and then is lifted moist adiabatically thereafter. The level of free convection (LFC) is the height where $\theta_{pcl} > \theta_{env}$, z_c is the level where $\theta_{pcl} = \theta_{env}$.

The CAPE is calculated for a pseudo-adiabatic process and a reversible moist adiabatic process, respectively, in this study. In the pseudo-adiabatic process, an air parcel is lifted adiabatically while all condensed water drops out from the parcel. In the reversible moist adiabatic process, an air parcel is lifted adiabatically while all condensed water is kept in the parcel. Following Xu and Emanuel (1989), The virtual temperatures (T_{vpa}) for the pseudo-adiabatic process and (T_{vre}) for the reversible moist adiabatic process are respectively expressed by

$$T_{vpa} = T_p \frac{1 + q_{vs}(T_p)/0.622}{1 + q_w}, \tag{13a}$$

and

$$T_{vre} = T_p \frac{1 + q_{vs}(T_p)/0.622}{1 + q_{vs}(T_p)}, \tag{13b}$$

where T_p is the temperature of a pseudo-adiabatically displaced air parcel; q_{vs} is the saturation specific humidity, and q_w is the total water content of the air parcel. $CAPE_{pa}$ for the pseudo-adiabatic process and $CAPE_{re}$ for the reversible moist adiabatic process are calculated by using (13a) and (13b), respectively.

3. Results

Figure 1 shows the time evolution of vertical distribution of the large-scale vertical velocity and zonal wind during 19-25 December 1992 that are imposed in the model. Strong upward motions with maxima of $15 - 25$ $mb\ hour^{-1}$ occur on late 20 December, and during the early mornings of 23 and 25 December between 400 and 500 mb. The latter two maxima are quasi-two-day oscillations (Takayabu et al. 1996) in the convective

phase of an intraseasonal oscillation during COARE. Two less intense upward motion centers appear during the nights of 19 and 21 December. The occurrence of maximum upward motion each night is consistent with the diurnal signals observed by Sui et al. (1997). The large scale zonal wind in the lower troposphere (below 700 mb) are westerly that strengthens to 10 ms^{-1} around 23 December. The mid-troposphere has an easterly-westerly wind oscillation with maximum easterly wind of -10 ms^{-1} at 500 mb on 20 December. The upper troposphere (above 250 mb) is dominated by easterly winds. As mentioned previously, the model is also forced by the observed horizontal temperature and moisture advections (not shown), which have much smaller amplitudes than the vertical advections respectively.

Figure 2a shows lag correlation coefficients between zonal-mean CAPE and rain rate. Positive lag hour denotes that CAPE leads rain rate. The maximum lag correlation coefficients between zonal-mean CAPE and rain rate indicate that the CAPE reaches maximum about 3-4 hours before the maximum rain rate. The minimum lag correlation coefficients indicate that the CAPE reaches minimum about 2 hour after the maximum rainfall. Both maximum and minimum are above 99% confidence level. The phase difference between maximum and minimum correlation coefficients is about 5 hours. Since a significant spectral peak appears at 9 hours by the power spectrum analysis of the hourly rain rate (not shown), the phase difference is about the half of the time scale of the simulated convection. Figure 2a also show that the lag correlation coefficients for $CAPE_{r\epsilon}$ and $CAPE_{pa}$ are similar.

Since the model is forced by imposed vertical velocity, the relationship between energy and imposed vertical velocity is first analyzed. Figure 2b shows lag correlation coefficients between $\overline{P}$ and $< \overline{w}^o >$ (solid line), and between K' and $< \overline{w}^o >$ (dashed line). Statistically significant lag correlation coefficients display that maximum K' lags imposed upward motion (positive $< \overline{w}^o >$) by 1-2 hours whereas minimum $\overline{P}$ lags upward motion by about 6 hours. This suggests that the K' leads $\overline{P}$ by about 4-5 hours, which is about the half of the time scale of the simulated convection. The statistically significant relationship can be also shown by lag correlation coefficients in Figure 3a that the imposed upward motion

leads minimum $\frac{\partial \overline{P}}{\partial t}$ (maximum decrease of horizontal-mean moist available potential energy) by 3 hours, whereas it lags maximum $\frac{\partial K'}{\partial t}$ (maximum increase of perturbation kinetic energy) by 1-2 hours. Thus, minimum $\frac{\partial \overline{P}}{\partial t}$ lags maximum $\frac{\partial K'}{\partial t}$ by 4-5 hours. The imposed large-scale upward motion with maximum $\frac{\partial K'}{\partial t}$ and K' indicates that convection is phase locked with the imposed large-scale upward motion. The negative lag correlation coefficient between $\frac{\partial \overline{P}}{\partial t}$ and $< \overline{w}^o >$ in Figure 3 means that the imposed large-scale downward motion leads maximum $\frac{\partial \overline{P}}{\partial t}$ by about 3 hours. Thus, the imposed downward motion results in a build up of $\overline{P}$, and provides a favorable environmental conditions for occurrence of convection.

The phase relation between $\frac{\partial \overline{P}}{\partial t}$ and $\frac{\partial K'}{\partial t}$ is also linked by local change of perturbation moist available potential energy $\frac{\partial P'}{\partial t}$. Minimum $\frac{\partial \overline{P}}{\partial t}$ lags minimum $\frac{\partial P'}{\partial t}$ by about 1 hour, and minimum $\frac{\partial P'}{\partial t}$ lags maximum $\frac{\partial K'}{\partial t}$ by about 3 hours (Fig. 3b), so that minimum $\frac{\partial \overline{P}}{\partial t}$ lags maximum $\frac{\partial K'}{\partial t}$ by about 4 hours. This is a statistically significant phase relation consistent to that shown in Figure 2b, although there are other two lag correlation coefficients between $\frac{\partial P'}{\partial t}$ and $\frac{\partial K'}{\partial t}$ that are above the 99 % confidence level. Two minimum lag correlation coefficients are 9-hour apart, indicative of the dominant life cycle of the model convective events. The maximum lag correlation coefficient appears between the two minimum lag correlation coefficients, indicating that $\frac{\partial P'}{\partial t}$ reaches maximum about one hour before maximum $\frac{\partial K'}{\partial t}$.

To further examine the dominant physical processes determining the phase relations, the lag correlation between each term of $\frac{\partial \overline{P}}{\partial t}$ [eq. (11)] and $\frac{\partial P'}{\partial t}$, and between $\frac{\partial \overline{P}}{\partial t}$ and each term of $\frac{\partial P'}{\partial t}$ [eq. (12)], and the lag correlation between each term of $\frac{\partial P'}{\partial t}$ [eq. (12)] and $\frac{\partial K'}{\partial t}$, and between $\frac{\partial P'}{\partial t}$ and each term of $\frac{\partial K'}{\partial t}$ [eq. (9)] are respectively plotted in Figures 4 and 5. Figure 4a shows that only the zero-hour lag correlation coefficient between $C_v(\overline{K}, \overline{P})$ and $\frac{\partial P'}{\partial t}$ is marginally around the 99 % confidence level, and above the 95 % confidence level. The term $C_v(\overline{K}, \overline{P})$ of $\frac{\partial \overline{P}}{\partial t}$ is a major component that contributes to the maximum positive zero-hour lag correlation between $\frac{\partial \overline{P}}{\partial t}$ and $\frac{\partial P'}{\partial t}$. The term $C_v(\overline{K}, \overline{P})$ is contributed by the vertical temperature and moisture advections respectively [see (11e)]. Further analysis shows that the lag correlation coefficient between vertical temperature

advection and imposed vertical velocity has the same sign with those between sum of vertical temperature and moisture advections and imposed vertical velocity, whereas the lag correlation coefficient between vertical moisture advection and imposed vertical velocity has the opposite sign (not shown). This indicates that vertical temperature advection determines the conversion term $C_v(\overline{K}, \overline{P})$. The imposed upward (downward) motion causes the vertically advective cooling (warming), which results in the loss (gain) of horizontal-mean moist available potential energy through the conversion term $C_v(\overline{K}, \overline{P})$. Figure 4a also shows that maximum zero-hour lag correlation coefficient between $G_{cn}(\overline{P})$ and $\frac{\partial P'}{\partial t}$ is slightly less than that between $C_v(\overline{K}, \overline{P})$ and $\frac{\partial P'}{\partial t}$. The conversion $G_{cn}(\overline{P})$ carries convective signals as shown in Figure 4a that the maximum lag correlation coefficient is about 9-hour apart.

Figure 4b shows that the lag correlation coefficients between $C(\overline{P}, P')$ and $\frac{\partial \overline{P}}{\partial t}$, and between $G_R(P')$ and $\frac{\partial \overline{P}}{\partial t}$, and between $G(P')$ and $\frac{\partial \overline{P}}{\partial t}$ are above 99 % confidence level. The terms $C(\overline{P}, P')$ and $G(P')$ have the same orders of magnitude (not shown), but they have the opposite signs (Fig. 4b) so that they cancel each other in large part. In addition, the amplitude of the term $C(K', P')$ is smaller than those of the terms $C(\overline{P}, P')$ and $G(P')$. As a result, the lag correlation coefficient between $C(\overline{P}, P') + G(P') + C(K', P')$ and $\frac{\partial \overline{P}}{\partial t}$ becomes statistically insignificant. This suggests that the vertical perturbation advection processes do not play important roles in determining phase of $\frac{\partial P'}{\partial t}$. Therefore, the term $G_R(P')$ makes that $\frac{\partial P'}{\partial t}$ leads $\frac{\partial \overline{P}}{\partial t}$ by about 1 hour. The radiative cooling with positive h' and radiative warming with negative h' cause the decrease of perturbation available potential energy through the conversion term $G_R(P')$.

Figure 5a shows that three maximum negative lag correlation coefficients and one maximum positive lag correlation coefficient are above 99 % confidence level. Again, small amplitude of $C(K', P')$ in contribution to $\frac{\partial P'}{\partial t}$, and cancelation between $C(\overline{P}, P')$ and $G(P')$ make the vertical perturbation advection processes less important in determining the phase of $\frac{\partial P'}{\partial t}$. The term $G_{cn}(P')$ plays a crucial role in controlling the phase of $\frac{\partial P'}{\partial t}$ as shown in Fig. 5a where the lag correlation coefficient between $G_{cn}(P')$ and $\frac{\partial K'}{\partial t}$ has the maximum negative value at -2 hour, and is statistically significant. This suggests that the

maximum loss of perturbation moist available potential energy and the maximum gain of perturbation kinetic energy are linked by the term $G_{cn}(P')$. Since $L_s > L_v$, the heating released by deposition with positive h' causes the loss of perturbation moist available potential energy. Maximum $G_{cn}(P')$ occurs about 3 hours after the maximum $\frac{\partial K'}{\partial t}$. It is important to notice that the maximum K' also occurs about 3 hours after the maximum $\frac{\partial K'}{\partial t}$ (Figs. 2b and 3a), indicating the minimum $G_{cn}(P')$ coincides with the strongest convection. Thus, the 3-hour of phase difference between $\frac{\partial P'}{\partial t}$ and $\frac{\partial K'}{\partial t}$ is the time length for convection developing to the strongest strength.

Figure 5b shows that the lag correlation correlation coefficients between $C(P', K')$ and $\frac{\partial P'}{\partial t}$ and between $G_{qv}(K')$ and $\frac{\partial P'}{\partial t}$ are similar, and their maximum negative values at -3 hours are barely above 99 % confidence level, which contribute to maximum negative lag correlation coefficient between $\frac{\partial P'}{\partial t}$ and $\frac{\partial K'}{\partial t}$ at -3 hours (Fig. 3b). The terms $G_{ql}(K')$ and $C(\overline{K}, K')$ have the opposite signs with the terms $C(P', K')$ and $G_{qv}(K')$ (Fig. 5b), the magnitude of $C(P', K')$ is larger than the other three terms (not shown) so that the term $C(P', K')$ determines $\frac{\partial K'}{\partial t}$. Covariance between the temperature and vertical velocity perturbations determines the local change of the perturbation kinetic energy. The thermally direct circulation of the upward motion with the higher temperature and the downward motion with the lower temperature converts the perturbation moist available potential energy to the perturbation kinetic energy, feeding the convection.

4. Discussion

Figure 6 summaries the phase relations between the convection and its embedding environment. The imposed large-scale downward motion yields a growth of $\overline{P}$ by the associated vertical advective warming $[C_v(\overline{K}, \overline{P}) > 0]$, building the favorable environment for occurrence of convection. The near simultaneous occurrence of maximum $\frac{\partial K'}{\partial t}$, K' , and large-scale upward motion, implying that convection is phase locked with the large-scale forcing. The life cycle of the simulated convective events (about 9 hours) is much shorter than the time scales of imposed large-scale forcing (longer than the diurnal cycle). In the

convective events, maximum $\frac{\partial K'}{\partial t}$ leads maximum $\frac{\partial P'}{\partial t}$ by about 3 hours through perturbation cloud heating $[G_{cn}(P')]$ and the vertical heat transport by perturbation circulations $[C(P', K')]$. Maximum $\frac{\partial K'}{\partial t}$ also leads maximum K' by about 3 hours, indicating that the 3-hour is the time required by convection to reach the maximum strength. Minimum $\frac{\partial P'}{\partial t}$ leads minimum $\frac{\partial \overline{P}}{\partial t}$ by about one hour through perturbation radiative processes $[G_R(P')]$ and the horizontal-mean cloud heating $[G_{cn}(\overline{P})]$, and the large-scale vertical advective cooling. Consequently, maximum $\frac{\partial K'}{\partial t}$ leads minimum $\frac{\partial \overline{P}}{\partial t}$ by 4-5 hours (about the half of the convective life scale).

The phase difference between perturbation kinetic energy associated with convection and its embedding environment associated with horizontal-mean moist available potential energy indicates that the generation of environmental unstable energy by large-scale processes is not simultaneously balanced by its destruction by convection. The minimum horizontal-mean moist available potential energy occurs 4-5 hours after maximum perturbation kinetic energy, and the phase lag is about the half of the convective time scale. This provides a concrete evidence for the adjustment from disequilibrium to quasi-equilibrium states proposed by Xu and Randall (1998). The results shows the convective time scale is related to the cloud microphysical processes, convective-radiative interactions, dynamic-thermodynamic coupling inside the convective system, suggesting that convective time scale (as well as the phase lag) may depend on characteristics of convection (cloud type). When the phase lag is included in cumulus parameterization, the convective time scale is introduced in the large-scale environment in the general circulation simulations. The scale interaction may have accumulated effects on the large-scale variabilities ranging from diurnal, intraseasonal, interannual time scales. This needs careful consideration in cumulus parameterization scheme, and more sensitivity experiments by the general circulation model.

5. Conclusion

Energetics analysis is carried out with a 2-D cloud resolving simulation to determine the physical processes responsible for the phase difference between convection and

its embedding environment. The cloud resolving model is forced by imposed time-varying horizontal-mean vertical velocity as well as zonal wind derived from the TOGA-COARE data set for a selective six day period. The imposed vertical velocity serves as external forcing in this particular model setup. Lag correlation analysis shows that the maximum perturbation kinetic energy associated with the simulated convective events and its maximum growth rate lags and leads the maximum imposed large-scale upward motion by about 1-2 hours respectively, indicating that the convection is phase locked with the imposed large-scale forcing. The imposed large-scale vertical velocity has the time scales longer than the diurnal cycle, whereas the simulated convective events have the dominant time scale of about 9 hours. The imposed large-scale upward motion leads to decrease the horizontal-mean moist available potential energy by the associated vertical advective cooling, providing the favorable environment for convection development.

With the maximum heating released by phase changes of cloud contents associated with the strongest convective events and the maximum vertical heat transport by perturbation circulations, maximum growth of perturbation kinetic energy leads maximum loss of perturbation available potential energy by about 3 hours. With the maximum vertical advective cooling associated with upward motion, the maximum horizontal-mean cloud related heating, and maximum perturbation radiative processes, maximum loss of perturbation moist available potential energy leads maximum loss of the horizontal-mean moist available potential energy by about one hour. Consequently, the maximum gain of perturbation kinetic energy leads the maximum loss of horizontal-mean moist available potential energy by about 4-5 hours (about the half of the time scale of life cycle of the simulated convection).

Acknowledgments. This research is supported under the TRMM project of NASA's Mission to Planet Earth Office.

APPENDIX

Relations used in derivation of energetics equations

The following relations are derived to obtain (9):

$$-<\overline{u'[\frac{\partial}{\partial x}(u'\overline{u}^o+\overline{u}^o u'+u'u')+\frac{1}{\overline{\rho}}\frac{\partial}{\partial z}\overline{\rho}(w'\overline{u}^o+\overline{w}^o u'+w'u'-\overline{w'u'})]}>$$

$$-<\overline{w'[\frac{\partial}{\partial x}(u'\overline{w}^o+\overline{u}^o w'+u'w')+\frac{1}{\overline{\rho}}\frac{\partial}{\partial z}\overline{\rho}(w'\overline{w}^o+\overline{w}^o w'+w'w'-\overline{w'w'})]}>$$

$$=-<\overline{(\overline{u}^o+u')\frac{\partial}{\partial x}\frac{[(u')^2+(w')^2]}{2}+(\overline{w}^o+w')\frac{\partial}{\partial z}\frac{[(u')^2+(w')^2]}{2}}>$$

$$-<\overline{u'w'}\frac{\partial\overline{u}^o}{\partial z}>-<\overline{w'w'}\frac{\partial\overline{w}^o}{\partial z}>$$

$$=-<\overline{u'w'}\frac{\partial\overline{u}^o}{\partial z}>-<\overline{w'w'}\frac{\partial\overline{w}^o}{\partial z}>, \qquad (A1)$$

$$-<\overline{c_p u'\frac{\partial}{\partial x}(\overline{\theta}\pi')+w'\frac{\partial}{\partial z}(\overline{\theta}\pi')}>=0, \qquad (A2)$$

where mass continuity and zero vertical velocity at top and bottom of the model atmosphere are applied. The following relations are derived to obtain (12):

$$-<\frac{\Gamma}{c_p}\overline{h'[\frac{\partial(u'h')}{\partial x}+\overline{u}^o\frac{\partial h'}{\partial x}+\frac{c_p\pi}{\overline{\rho}}\frac{\partial}{\partial z}\overline{\rho}w'\theta'+c_p\pi\overline{w}^o\frac{\partial\theta'}{\partial z}+\frac{L_v}{\overline{\rho}}\frac{\partial}{\partial z}\overline{\rho}w'q_v'+L_v\overline{w}^o\frac{\partial q_v'}{\partial z}]}>$$

$$=-<\frac{\Gamma}{c_p}\overline{h'[(\overline{u}^o+u')\frac{\partial h'}{\partial x}+(\overline{w}^o+w')(c_p\pi\frac{\partial\theta'}{\partial z}+L_v\frac{\partial q_v'}{\partial z})]}>$$

$$=-<\frac{\Gamma}{c_p}\overline{h'[(\overline{u}^o+u')\frac{\partial h'}{\partial x}+(\overline{w}^o+w')\frac{\partial h'}{\partial z}-c_p(\overline{w}^o+w')\theta'\frac{\partial\pi}{\partial z})]}>$$

$$=-<\frac{\Gamma}{c_p}\overline{[\frac{\partial}{\partial x}(\overline{u}^o+u')\frac{(h')^2}{2}+\frac{\partial}{\overline{\rho}\partial z}\overline{\rho}(\overline{w}^o+w')\frac{(h')^2}{2}-c_p(\overline{w}^o+w')\theta'\frac{\partial\pi}{\partial z}]}>$$

$$=-<\frac{\Gamma}{2c_p}\frac{\partial}{\overline{\rho}\partial z}[\overline{\rho(\overline{w}^o+w')(h')^2}]>-<\frac{g\Gamma}{c_pT_b}\overline{(\overline{w}^o+w')T'h'}>, \qquad (A3)$$

$$-<\frac{\Gamma}{c_p}\overline{h'(c_p\pi w'\frac{\partial\overline{\theta}}{\partial z}+L_v w'\frac{\partial\overline{q}_v}{\partial z})}>$$

$$=-<\frac{\Gamma}{c_p}[c_p\pi\frac{\partial}{\partial z}(\overline{\theta}-\theta_b)+L_v\frac{\partial}{\partial z}(\overline{q}_v-q_{vb})]\overline{w'h'}>+<\frac{\Gamma}{c_p}(c_p\pi\frac{\partial\theta_b}{\partial z}+L_v\frac{\partial q_{vb}}{\partial z})\overline{w'h'}>$$

$$= - < \frac{\Gamma}{c_p}\overline{w'h'}[\frac{\partial}{\partial z}(\overline{h}-h_b) - c_p(\overline{\theta}-\theta_b)\frac{\partial \pi}{\partial z}] > + < \frac{\Gamma}{c_p}(c_p\pi\frac{\partial \theta_b}{\partial z} + L_v\frac{\partial q_{vb}}{\partial z})\overline{w'h'} >$$

$$= - < \frac{\Gamma}{c_p}\frac{\partial}{\overline{\rho}\partial z}\overline{\rho}(\overline{h}-h_b)\overline{w'h'} > + < \frac{\Gamma}{c_p}(\overline{h}-h_b)\frac{\partial}{\overline{\rho}\partial z}\overline{\rho w'h'} > - < \frac{g\Gamma}{c_pT_b}(\frac{\overline{T}}{T_b}-1)\overline{h'w'} >$$

$$- < g\frac{\overline{w'T'}}{T_b} > - < \frac{gL_v}{c_pT_b}\overline{w'q_v'} >$$

$$= - < \frac{\Gamma}{c_p}\frac{\partial}{\overline{\rho}\partial z}\overline{\rho}(\overline{h}-h_b)\overline{w'h'} > + < \frac{\Gamma}{c_p}(\overline{h}-h_b)(c_p\pi\frac{\partial}{\overline{\rho}\partial z}\overline{\rho w'\theta'} + L_v\frac{\partial}{\overline{\rho}\partial z}\overline{\rho w'q_v'}) >$$

$$- < \frac{g\Gamma}{c_pT_b}(\overline{h}-h_b)\overline{T'w'} > - < \frac{g\Gamma}{c_pT_b}(\frac{\overline{T}}{T_b}-1)\overline{h'w'} > - < g\frac{\overline{w'T'}}{T_b} > - < \frac{gL_v}{c_pT_b}\overline{w'q_v'} > . \quad (A4)$$

References

Arakawa, A., W. H. Schubert, 1974: Interaction of a cumulus cloud ensemble with the large-scale environment. Part I. *J. Atmos. Sci.*, **31**, 674-701.

Betts, A. K., and M. J. Miller, 1986: A new convective adjustment scheme. Part II: Single column tests using GATE wave, BOMEX, ATEX and arctic airmass data sets. *Quart. J. Roy. Meteor. Soc.*, **112**, 692-709.

Cheng, M.-D., and M. Yanai, 1989: Effects of downdrafts and mesoscale convective organization on the heat and moisture budgets of tropical cloud clusters Part III: Effects of mesoscale convective organization. *J. Atmos. Sci.*, **46**, 1566-1588.

Lorenz, E. N., 1978: Available potential energy and the maintenance of the general circulation. *Tellus*, **30**, 15-31.

Lorenz, E. N., 1979: Numerical evaluation of moist available energy. *Tellus*, **31**, 230-235.

Li, X., C.-H. Sui, K.-M. Lau, and M.-D. Chou, 1999: Large-scale forcing and cloud-radiation interaction in the tropical deep convective regime. *J. Atmos. Sci.*, **56**, 3028-3042.

Manabe, S., and R. F. Strickler, 1964: Thermal equilibrium of the atmosphere with a convective adjustment. *J. Atmos. Sci.*, **21**, 361-385.

Randall, D. A., and J. Wang, 1992: The moist available energy of a conditionally unstable atmosphere. *J. Atmos. Sci.*, **49**, 240-255.

Randall, D. A., and D.-M. Pan, 1993: Implementation of the Arakawa-Schubert cumulus parameterization with a prognostic closure. *The Representation of Cumulus Convection in Numerical Models of the Atmosphere*, K. A. Emannuel and D. J. Raymond, Eds. *Meteor. Monogr.*, No. 46, 37-144.

Soong, S. T., and Y. Ogura, 1980: Response of tradewind cumuli to large-scale processes. *J. Atmos. Sci.*, **37**, 2035-2050.

Soong, S. T., and W. K. Tao, 1980: Response of deep tropical cumulus clouds to mesoscale processes. *J. Atmos. Sci.*, **37**, 2016-2034.

Sui, C.-H., K.-M. Lau, Y. Takayabu, and D. Short, 1997: Diurnal variations in tropical oceanic cumulus ensemble during TOGA COARE. *J. Atmos. Sci.*, **54**, 639-655.

Sui, C.-H., X. Li, and K.-M. Lau, 1998: Radiative-convective processes in simulated diurnal variations of tropical oceanic convection. *J. Atmos. Sci.*, **55**, 2345-2359.

Takayabu, Y. N., K.-M. Lau, and C.-H. Sui, 1996: Observation of a quasi-2-day wave during TOGA COARE. *Mon. Wea. Rev.*, **124**, 1892-1913.

Tao, W.-K., and J. Simpson, 1993: The Goddard Cumulus Ensemble model. Part I: Model description. *Terr. Atmos. Oceanic Sci.*, **4**, 35-72.

Thompson, R. M., Jr., S. W. Payne, E. E. Recker, and R. J. Reed, 1979: Structure and properties of synoptic-scale wave disturbances in the intertropical convergence zone of the eastern Atlantic. *J. Atmos. Sci.*, **36**, 53-72.

Wang, J., and D. A. Randall, 1994: The moist available energy of a conditionally unstable atmosphere. Part II: Further analysis of GATE data. *J. Atmos. Sci.*, **51**, 703-710.

Xu, K.-M., and K. A. Emanuel, 1989: Is the tropical atmosphere conditionally unstable? *Mon. Wea. Rev.*, **117**, 1471-1479.

Xu, K.-M., and D. A. Randall, 1998: Influence of large-scale advective cooling and moistening effects on the quasi-equilibrium behavior of explicitly simulated cumulus ensembles. *J. Atmos. Sci.*, **55**, 896-909.

Figure Captions

Fig. 1 Time evolution of (a) vertical velocity ($mb\ hour^{-1}$), and (b) zonal wind (ms^{-1}) taken from the TOGA COARE (Sui et al. 1997) for a six-day period. Downward motion in (a) and westerly wind in (b) are shaded.

Fig. 2 Lag correlation coefficients between horizontal-mean CAPE and rain rate in (a), and between $\overline{P}$ and $< \overline{w}^o >$ (solid) and between K' and $< \overline{w}^o >$ (dashed) in (b). Solid and dashed lines in (a) denote cases for a pseudo-adiabatic process and a reversible moist adiabatic process respectively. Lag correlation coefficient curves above upper light dot line or below lower light dot line exceed 99 % confidence level.

Fig. 3 Lag correlation coefficients between $\frac{\partial \overline{P}}{\partial t}$ and $< \overline{w}^o >$ (solid) and between $\frac{\partial K'}{\partial t}$ and $< \overline{w}^o >$ (dashed) in (a), and between $\frac{d\overline{P}}{\partial t}$ and $\frac{\partial P'}{\partial t}$ (solid) and between $\frac{\partial P'}{\partial t}$ and $\frac{\partial K'}{\partial t}$ (dashed) in (b). Lag correlation coefficient curves above upper light dot line or below lower light dot line exceed 99 % confidence level.

Fig. 4 Lag correlation coefficients between each term of $\frac{\partial \overline{P}}{\partial t}$ [Eq. (11)] and $\frac{\partial P'}{\partial t}$ in (a), and between $\frac{\partial \overline{P}}{\partial t}$ and each term of $\frac{\partial P'}{\partial t}$ [Eq. (12)] in (b). Lag correlation coefficient curves above upper light dot line or below lower light dot line exceed 99 % confidence level.

Fig. 5 Lag correlation coefficients between each term of $\frac{\partial P'}{\partial t}$ [Eq. (12)] and $\frac{\partial K'}{\partial t}$ in (a), and between $\frac{\partial P'}{\partial t}$ and each term of $\frac{\partial K'}{\partial t}$ [Eq. (9)] in (b). Lag correlation coefficient curves above upper light dot line or below lower light dot line exceed 99 % confidence level.

Fig. 6 Schematic diagram for the summary of phase relationship between the convection and its embedding environment in term of $\frac{\partial \overline{P}}{\partial t}$, $\frac{\partial P'}{\partial t}$, and $\frac{\partial K'}{\partial t}$.

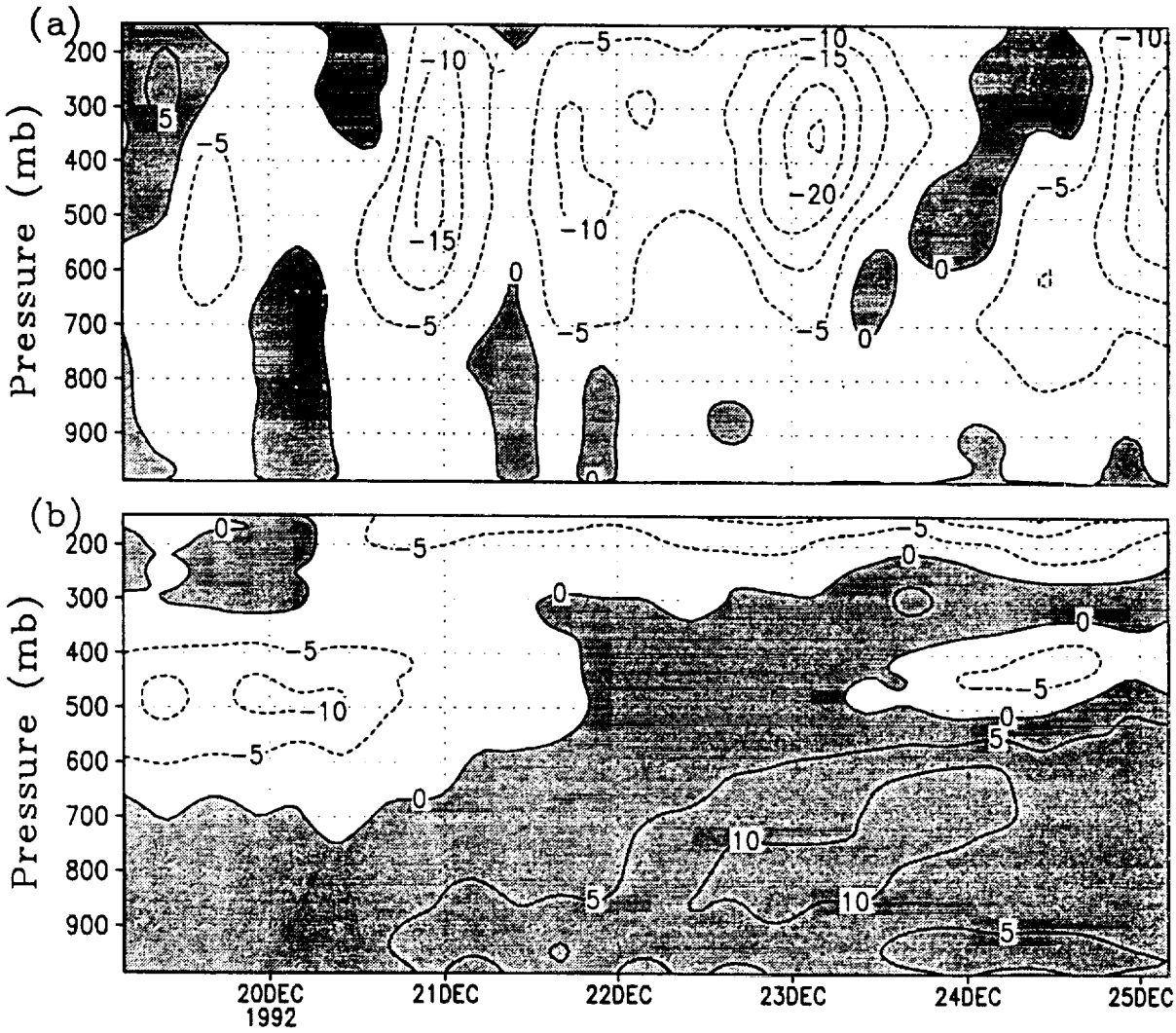
(a)
(b)
Pressure (mb)
200
300
400
500
600
700
800
900
20DEC
1992
21DEC
22DEC
23DEC
24DEC
25DEC

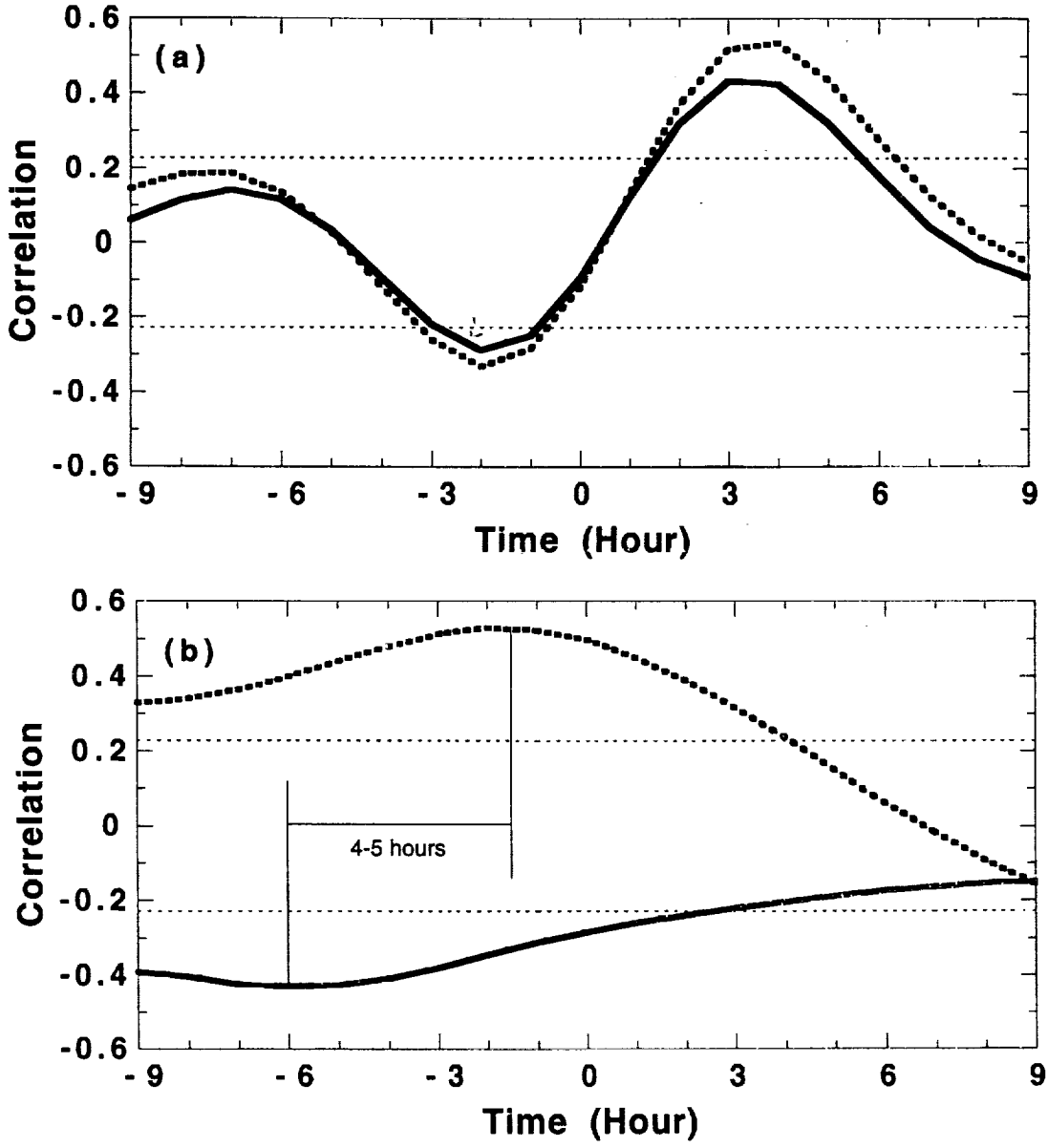
(a)
0.6
0.4
0.2
0
-0.2
-0.4
-0.6
Correlation
- 9
- 6
- 3
0
3
6
9
Time (Hour)
(b)
4-5 hours
Correlation
Time (Hour)

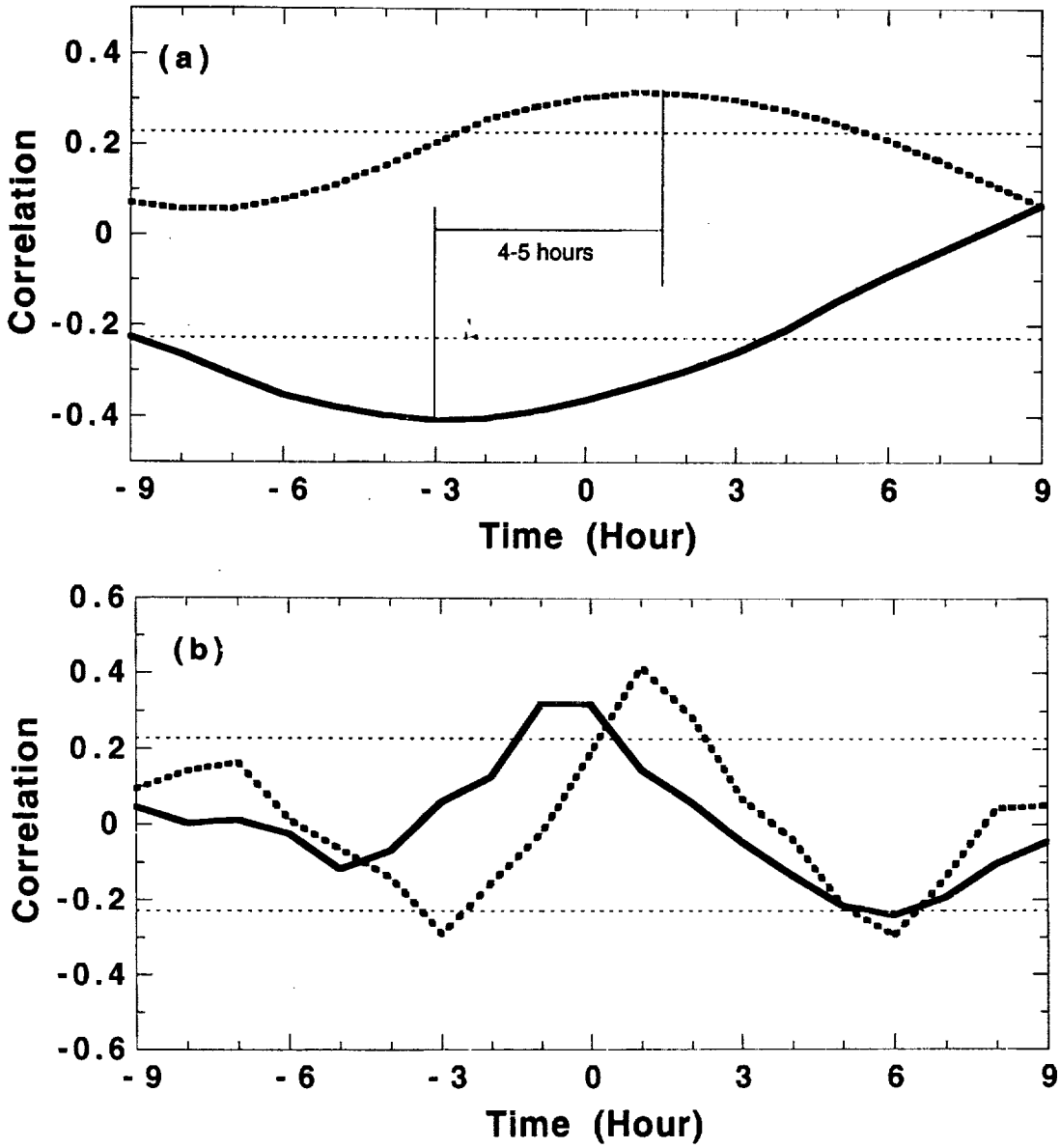
(a)
0.4
0.2
0
-0.2
-0.4
Correlation
4-5 hours
- 9
- 6
- 3
0
3
6
9
Time (Hour)
(b)
0.6
0.4
0.2
0
-0.2
-0.4
-0.6
Correlation
- 9
- 6
- 3
0
3
6
9
Time (Hour)

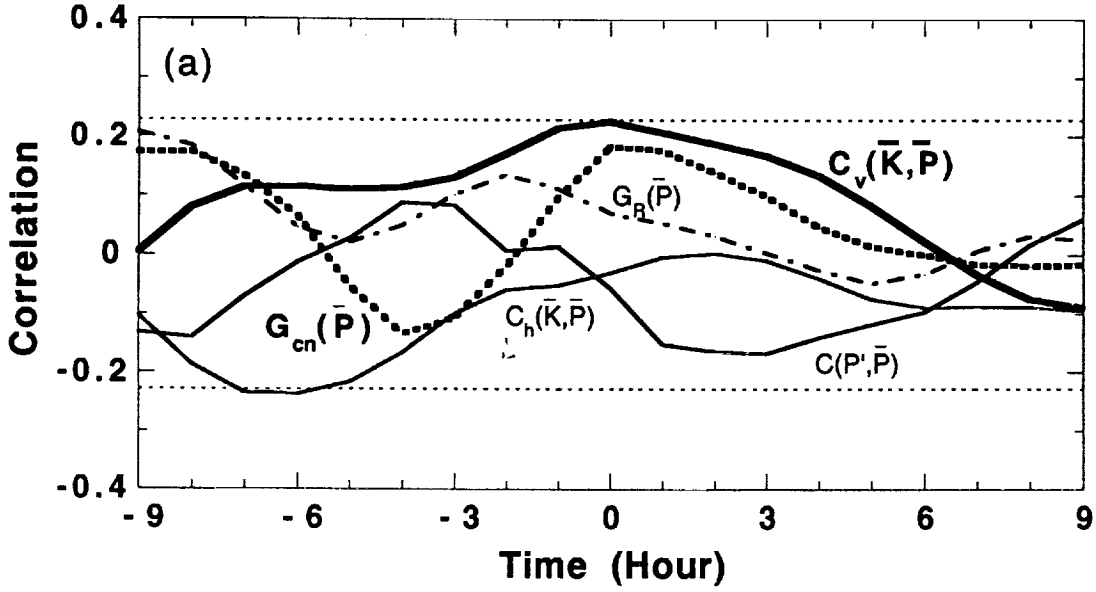
(a)
0.4
0.2
0
-0.2
-0.4
Correlation
- 9
- 6
- 3
0
3
6
9
Time (Hour)
$C_v(\bar{K},\bar{P})$
$G_R(\bar{P})$
$G_{cn}(\bar{P})$
$C_h(\bar{K},\bar{P})$
$C(P',\bar{P})$

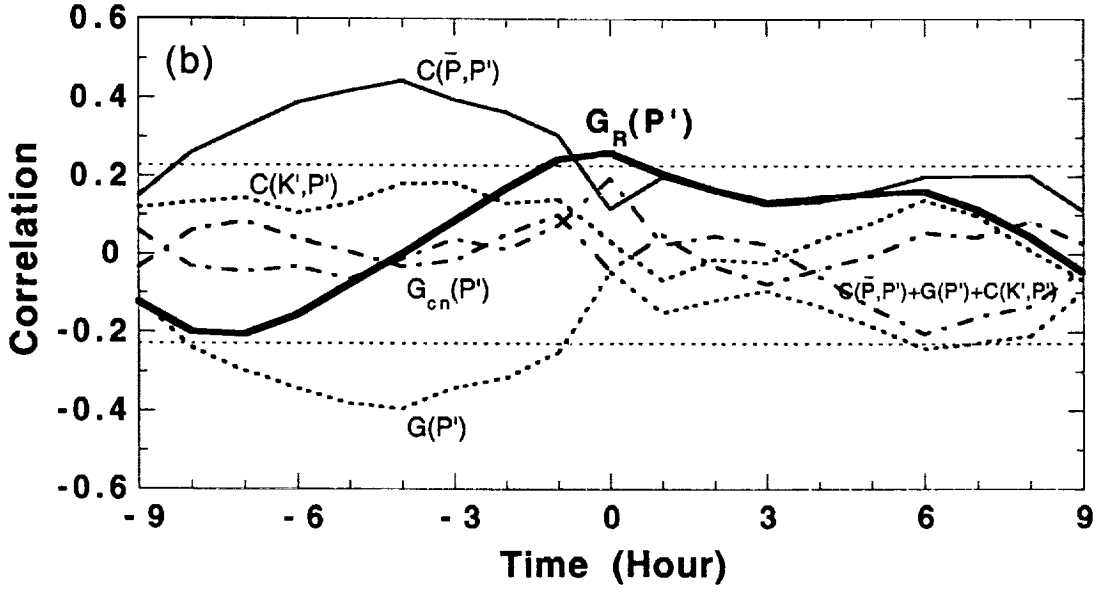
(b)
0.6
0.4
0.2
0
-0.2
-0.4
-0.6
Correlation
- 9
- 6
- 3
0
3
6
9
Time (Hour)
$C(\bar{P},P')$
$G_R(P')$
C(K',P')
$G_{cn}(P')$
$C(\bar{P},P')+G(P')+C(K',P')$
G(P')

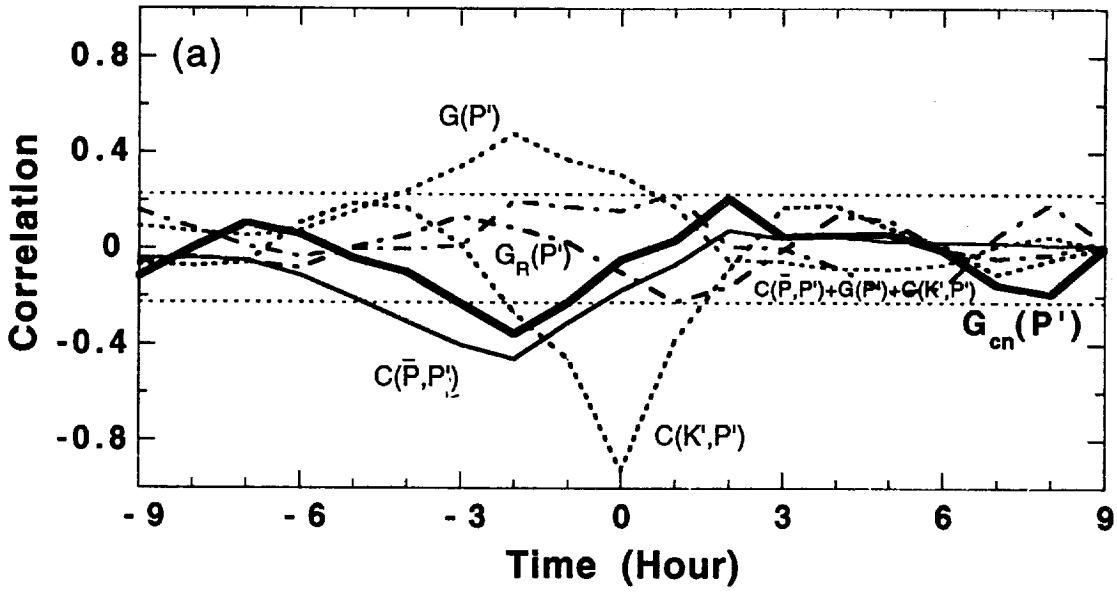
(a)
0.8
0.4
0
-0.4
-0.8
Correlation
G(P')
$G_R(P')$
$C(\bar{P},P')+G(P')+C(K',P')$
$G_{cn}(P')$
$C(\bar{P},P')$
C(K',P')
-9
-6
-3
0
3
6
9
Time (Hour)

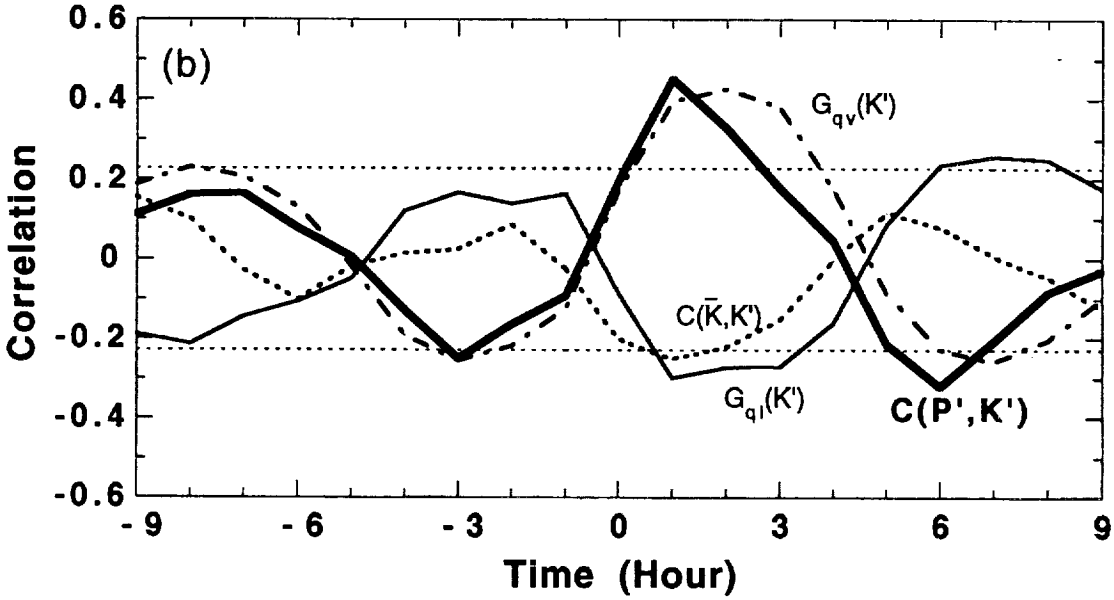
(b)
0.6
0.4
0.2
0
-0.2
-0.4
-0.6
Correlation
$G_{qv}(K')$
$C(\bar{K},K')$
$G_{ql}(K')$
C(P',K')
-9
-6
-3
0
3
6
9
Time (Hour)

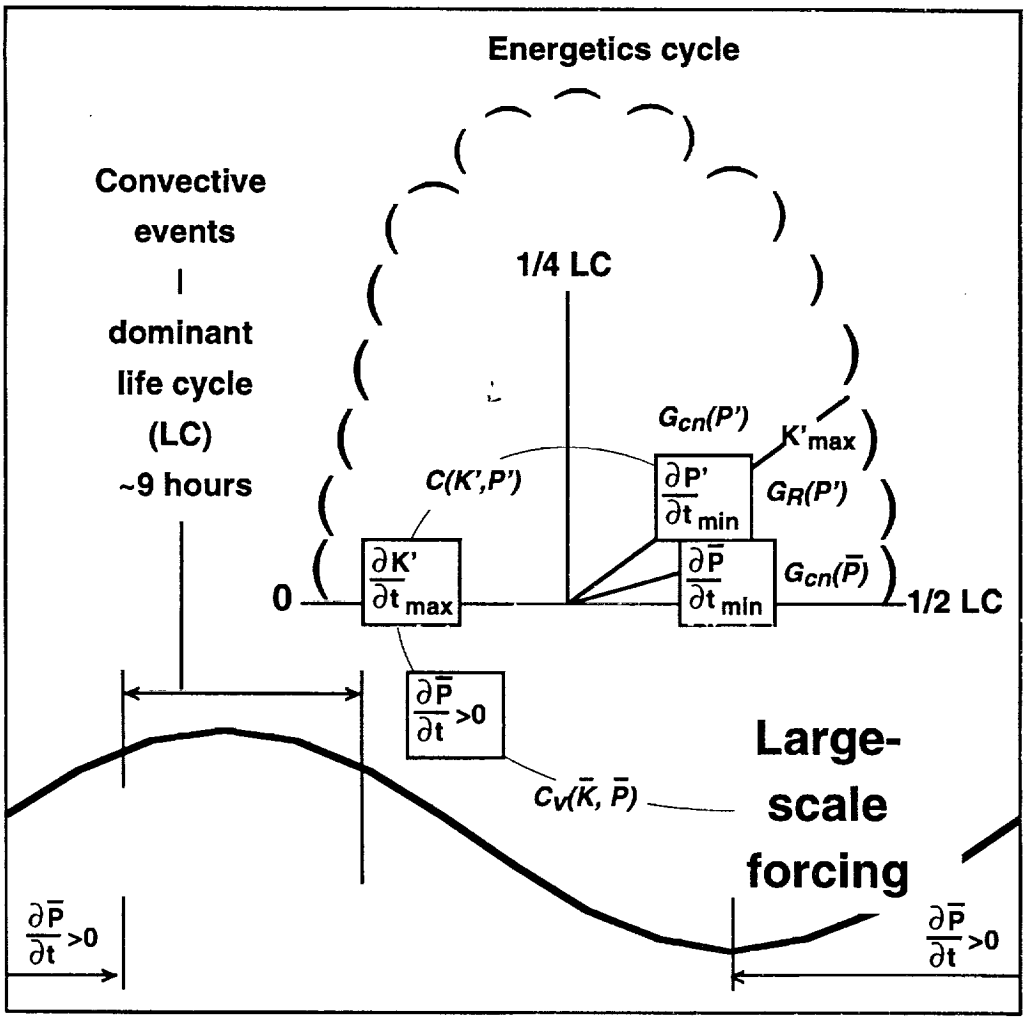
Energetics cycle
Convective events | dominant life cycle (LC) ~9 hours
1/4 LC
$G_{cn}(P')$
K'max
$C(K',P')$
$\frac{\partial P'}{\partial t}_{min}$
$G_R(P')$
$\frac{\partial K'}{\partial t}_{max}$
$\frac{\partial \bar{P}}{\partial t}_{min}$
$G_{cn}(\bar{P})$
0
1/2 LC
$\frac{\partial \bar{P}}{\partial t}>0$
$C_V(\bar{K}, \bar{P})$
Large-scale forcing
$\frac{\partial \bar{P}}{\partial t}>0$
$\frac{\partial \bar{P}}{\partial t}>0$